Journal of Controlled Release 308 (2019) 44–56

Contents lists available at ScienceDirect

Journal of Controlled Release

journal homepage: www.elsevier.com/locate/jconrel

Coated cationic lipid-nanoparticles entrapping miR-660 inhibit tumor growth in patient-derived xenografts lung cancer models

Massimo Moro[a,1], Daniela Di Paolo[b,1], Massimo Milione[c], Giovanni Centonze[a], Viviana Bornaghi[a], Cristina Borzi[a], Paolo Gandellini[d], Patrizia Perri[b], Ugo Pastorino[e], Mirco Ponzoni[b], Gabriella Sozzi[a,2], Orazio Fortunato[a,2,*]

[a] Tumor Genomics Unit, Department of Research, Fondazione IRCCS Istituto Nazionale dei Tumori, 20133 Milan, Italy
[b] Laboratory of Experimental Therapy in Oncology, IRCCS Istituto Giannina Gaslini, 16147 Genoa, Italy
[c] Anatomic Pathology Unit, Department of Pathology and Laboratory Medicine, Fondazione IRCCS Istituto Nazionale dei Tumori, 20133 Milan, Italy
[d] Department of Biosciences, University of Milan, Milan 20133, Italy
[e] Thoracic Surgery Unit, Fondazione IRCCS Istituto Nazionale dei Tumori, 20133 Milan, Italy

ARTICLE INFO

Keywords:
microRNA
Lung cancer
Lipid-nanoparticles
P53
Patient-derived xenografts

ABSTRACT

Lung cancer is the leading cause of cancer-related deaths. Late diagnosis and inadequate therapies contribute to poor outcomes. MicroRNAs (miRNAs) are small non-coding RNAs and are involved in lung cancer development. Because miRNAs simultaneously regulate several cancer-related genes, they represent an interesting therapeutic approach for cancer treatment. We have developed Coated Cationic Lipid-nanoparticles entrapping miR-660 (CCL660) and intraperitoneally administered (1.5 mg/Kg) twice a week for four weeks into SCID mice carrying subcutaneously lung cancer Patients Derived Xenografts (PDXs). Obtained data demonstrated that miR-660 is down-regulated in lung cancer patients and that its replacement inhibited lung cancer growth by inhibiting the MDM2-P53 axis. Furthermore, systemic delivery of CCL660 increased miRNA levels in tumors and significantly reduced tumor growth in two different P53 wild-type PDXs without off-target effects. MiR-660 administration reduced cancer cells proliferation by inhibiting MDM2 and restoring P53 function and its downstream effectors such as p21. Interestingly, anti-tumoral effects of CCL660 also in P53 mutant PDXs but with a functional p21 pathway were observed. Stable miR-660 expression inhibited the capacity of H460 metastatic lung cancer cells to form lung nodules when injected intravenously into SCID mice suggesting a potential role of miR-660 in metastatic dissemination.

To investigate the potential toxic effects of both miRNAs and delivery agents, an *in vitro* approach revealed that miR-660 replacement did not induce any changes in both mouse and human normal cells. Interestingly, lipid-nanoparticle delivery of synthetic miR-660 had no immunological off-target or acute/chronic toxic effects on immunocompetent mice. Altogether, our results highlight the potential role of coated cationic lipid-nanoparticles entrapping miR-660 in lung cancer treatment without inducing immune-related toxic effects.

1. Introduction

Lung cancer is a disease with a poor prognosis, accounting for 20% of total cancer-related deaths in Europe [1]. The majority of lung cancers are represented by the non-small cell lung cancer (NSCLC) subtype that has a 5-year survival rate of < 18% [2]. Currently, surgical resection is the most common treatment for early-stage tumors and is combined with chemotherapeutic agents for patients with advanced lung cancer; chemotherapy alone is used for patients with metastatic disease [3]. Platinum-based treatment is commonly used in clinical practice, with a small effect on improving the survival of patients with lung cancer [4]. The discovery of activating mutations in the *EGFR* gene (23%) and rearrangements in the anaplastic lymphoma kinase (*ALK*) gene (3–7%) [5] had a relevant impact on the treatment of patients with lung cancer, based on their responsiveness to tyrosine kinase inhibitors (TKIs), such as erlotinib, crizotinib and gefitinib [6,7]. Recently, pembrolizumab was approved as a first-line treatment for patients with lung cancer expressing high levels of programmed cell death

* Corresponding author.
E-mail address: orazio.fortunato@istitutotumori.mi.it (O. Fortunato).
[1] These authors contributed equally to this work.
[2] These authors contributed equally to this work.

https://doi.org/10.1016/j.jconrel.2019.07.006
Received 29 January 2019; Received in revised form 3 July 2019; Accepted 7 July 2019
Available online 09 July 2019

ligand 1 (PD-L1) [8]. Unfortunately, targeted therapies and pembrolizumab represent the first-line treatments for only 30% of patients [9]. Thus, the identification of novel treatment strategies remains a critical and essential need for lung cancer management.

The tumor suppressor gene *P53* plays an important role in preventing cancer development and is mutated/deleted in 50% of NSCLC cases [10]. *P53* activity is finely controlled and, among *P53* modulators, mouse double minute 2 (MDM2) plays an important role [11]. Furthermore, MDM2 function is linked to *P53* through an autoregulatory feedback loop under both normal and pathological conditions [12,13]. Based on these considerations, strategies that restore P53 function by inhibiting MDM2 represent a potential therapy for *P53* wild-type lung cancers [14].

MicroRNAs (miRNAs) are small non-coding, 22 nucleotides long RNAs that bind complementary sequences of target mRNAs to induce their degradation or repress translation [15]. Recent studies have reported altered expression patterns of miRNAs in several human malignancies, including lung cancer [16]. The revelation that miRNAs function as potential oncogenes and tumor suppressors has generated great interest in using them as targets for cancer therapy [17]. We previously identified miR-660 as a tumor suppressor miRNA in lung cancer cells. The replacement of this miRNA inhibits the migration and invasion of tumor cells and blocks tumor growth both *in vitro* and *in vivo*. The anti-tumor effects are mediated by MDM2 downregulation and activation of the P53 pathway [18].

The roles of miRNAs as novel therapeutic agents have received increasing attention [19]. Although several pre-clinical studies examining miRNAs have been conducted over the years, only a few have transitioned into clinical development. Several obstacles must be overcome to envisage the clinical use of miRNA therapy. These challenges include the design of optimal miRNA delivery vehicles with higher stability or reduction of off-target effects and toxicity [20].

Several delivery methods, such as nanoparticles, viral vectors and liposomes, are available to restore the expression of tumor suppressor miRNAs [21]. Due to their size and hydrophobic and hydrophilic characters (in addition to biocompatibility), liposomes represent a promising system for miRNA delivery because they protect and deliver nucleic acids and exhibit reduced toxicity and an improved therapeutic index [22,23]. Because Coated Cationic Lipid-nanoparticles (CCL) carriers have been shown to efficiently deliver asODNs/siRNAs/miRNAs [24–27], in the present study, we generated novel lipidic nanoparticles entrapping miRNA-660 (CCL660) as a lung cancer treatment to explore its potential for inhibiting lung cancer cell growth.

Thus, we aimed to i) evaluate the anti-tumor activity of CCL660 in patient-derived xenograft (PDX) models of lung cancer [28]; ii) elucidate the mechanism of action of CCL-delivered miR-660 within tumor cells; and iii) evaluate the acute and chronic toxicity of this lipid-nanoparticles formulation in mouse models.

2. Results

2.1. Characterization of Coated Cationic Lipid-nanoparticles (CCL) entrapping miRNAs

The CCLs were designed according to the number of negative charges of the miRNA sequence, obtaining a miRNA entrapment efficiency of approximately 85–90%. Lipid-nanoparticles possess a mean hydrodynamic diameter of 121 ± 6 nm for CCL660 and 123 ± 5 nm for CCLSCR, with a mean polydispersity index (PdI) of 0.092 ± 0.018 for CCL660 and 0.095 ± 0.019 for CCLSCR, indicating that we obtained a good monodisperse preparation (Table 1). Moreover, the two formulations presented similar *Z*-potentials in water and PBS [24,29,30] (CCL660: −17.1 ± 3.1 mV and − 2.3 ± 0.3 mV and CCLSCR: −18.5 ± 1.3 mV and − 1.6 ± 0.2, respectively), indicating good stability in medium resembling physiological conditions (Table 1). These parameters warrant and justify the loss of aggregation during lipid-nanoparticles storage and increase the half-life under systemic conditions, as expected due to the presence of the polyethylene glycol (PEG) shield [31].

Table 1
Physico-chemical characterization of CCLs.

Sample	Size		*Z*-potential [mV]	
	Diameter [nm]	PdI	H_2O	PBS
CCLSCR	123 ± 5	0.095 ± 0.019	−18.5 ± 1.3	−1.6 ± 0.2
CCL660	121 ± 6	0.092 ± 0.018	−17.1 ± 3.1	−2.3 ± 0.3

Table 1 The sizes and Z-potentials of CCLSCR and CCL660 were determined using a particle size analyzer. The PdI indicates the homogeneity of the samples in terms of size distribution. The value ranges from zero (good preparation) to one (bad formulation). Z-potential in H_2O represents the real charge of the particles, as well as their aggregation potential. Z-potential in PBS indicates the charge of the particles under physiological conditions. The results are presented as means of triplicate reading of each lipid-nanoparticles ± standard deviations.

2.2. CCL660 administration reduces tumor growth in P53 wild type models

We subcutaneously implanted PDX samples into SCID mice and assessed the miRNA biodistribution after 1 (at $t = 24$ h after tumor implantation) or 2 (at t = 24 h and $t = 96$ h after tumor implantation) intravenous (*i.v.*) or intraperitoneal (*i.p.*) injections of CCLs (1.5 mg/Kg) ($n = 3$ animals per group) to evaluate the efficacy of the delivery of the lipidic miRNA nanoparticles. The digital PCR (dPCR) analysis revealed 4- and 3-fold increases in the miRNA levels in tumors after single *i.p.* and *i.v.* injections, respectively. The double treatment confirmed the presence of higher levels of the liposomal compound both in tumors and plasma than in untreated animals (Fig. S1).

Next, we tested the efficacy of the CCL660 treatment in PDX305, PDX73 (both *P53wt*) and PDX111 (*P53mut*) by administering the miRNA entrapped in the lipidic-nanoparticles formulation (1.5 mg/Kg) *i.p.* twice a week for four weeks. The PDX samples were subcutaneously implanted into SCID mice, and treatment was started when the tumors reached 100–150 mm^3 in volume (7/8 days after cell inoculation). Interestingly, an appreciable reduction in tumor volume was observed at 42 days in *P53wt* PDXs (25% for PDX305 and 47% for PDX73 reduction in the volume of CCL660-treated tumors compared with that of vehicle-treated tumors, Fig. 1A-B), whereas the *P53*-mutated PDX111 was not affected by the CCL660 treatment (Fig. 1A-B). Furthermore, we treated PDX models also with lipid-nanoparticles encapsulating a negative-scrambled sequence (CCLSCR) to confirm that the anti-tumor effects of CCL660 were due to miR-660 activity without observing variation in tumor growth compared with the HEPES controls ($n = 4$ animals per PDX305 and PDX11; $n = 6$ for PDX73) (Fig. 1A-B).

Based on these data, the lipidic-nanoparticles miRNA formulation reached PDXs growing subcutaneously in immunocompromised mice, and CCL660 impaired tumor growth in a P53-dependent manner.

2.3. CCL660 induces cell cycle arrest by modulating MDM2 levels

We examined miR-660 expression in mouse organs and tumor cells using dPCR to determine whether the anti-tumor activity of the miRNA was responsible for the observed reduction in tumor growth. In CCL660-treated tumors, miR-660 expression was increased by 20-, 5- and 2.5-fold compared with that in control mice, in PDX305, PDX73 and PDX111, respectively (Fig. 2A). In addition, miRNA accumulation was observed in the liver, lung, spleen and plasma, consistent with the findings of previous miRNA delivery studies [32] (Fig. 2A).

Moreover, miRNA *in situ* hybridization (ISH) analysis confirmed an increase in miR-660 expression in CCL660-treated tumors compared with that in controls (CCLSCR- and vehicle- treated) tumors in both

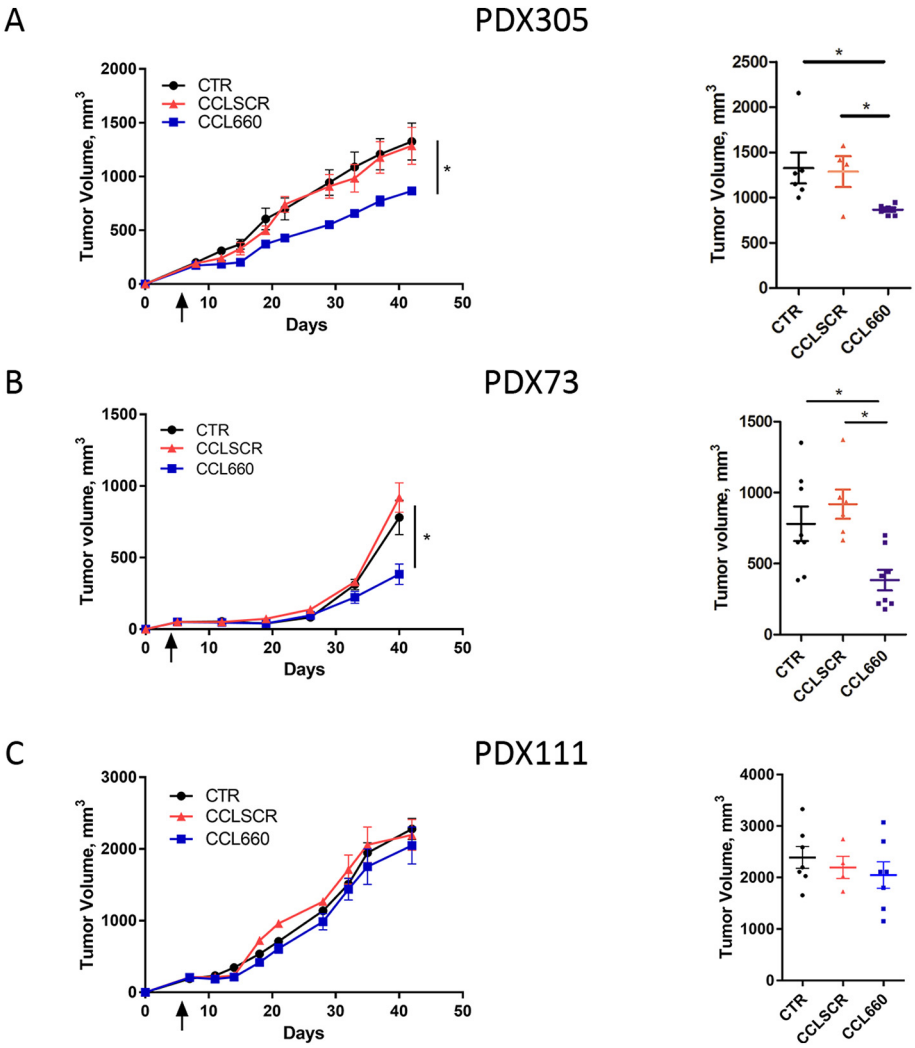

Fig. 1. CCL660 reduces tumor growth in P53wt models. **A**) Tumor growth curves of PDX305 (n = 6 for CTR and CCL660, n = 4 for CCLSCR, left panel), PDX73 (n = 8 for CTR and CCL660, n = 6 for CCLSCR centre panel) and PDX111 (n = 7 for CTR and CCL660, n = 4 for CCLSCR, right panel) treated with CCL660 (1.5 mg/kg) for 4 weeks. The black arrow indicates the day on which treatment began **B**) Graphs show the tumor volumes at the end of CCL660 treatment (42 days) compared with those in control mice (both CTR and CCLSCR). Data are presented as means ± S.E.M. * $p < .05$ (One-way ANOVA test comparing CCL660 *vs* CTR or CCLSCR).

PDX models (28%,30% and 26% miR-660-positive cells in animals treated for PDX305, PDX73 and PDX111, respectively, compared with 10% endogenous miR-660-positive cells in the controls (CTR and CCLSCR) for both models; $p < .05$) (Fig. 2B and Fig. S2). Immunohistochemical (IHC) staining for Ki-67 was evaluated at 42 days and showed a reduction in the mitotic index of CCL660-treated tumors compared with that of the controls, according to the *P53* status (32%,15% and 0% reduction in the number of Ki-67-positive cells in PDX305, PDX73 and PDX111, respectively) (Fig. 2B and Fig. S2).

Since the *MDM2* mRNA is a direct target of miR-660, we evaluated *MDM2* expression using real-time PCR and observed 40%, 80% and 50% reductions in PDX305, PDX73 and PDX111, respectively (Fig. 2C). A concomitant increase in *P53* and *P21* mRNA expression was observed in *P53wt* CCL660-treated tumors compared to controls ($p < .05$). Despite the observed *MDM2* down-regulation in PDX111 (*P53mut* model), *P21* transcription was not affected, confirming that a wild-type *P53* gene is required for the anti-tumor activity of miR-660 (Fig. 2C). The modulation of MDM2/P53 axis after CCL660 was confirmed by IHC analysis showing MDM2 modulation and P53 and P21 up-regulation (Fig. 2D and Fig. S2). MDM2 protein was not detected by IHC in PDX305 and PDX111 as already described [33].

2.4. Long- lasting treatment increases the CCL660-mediated inhibition of tumor growth

We treated another *PDX* model, PDX302, carrying a *P53* mutation responsible for P53 trafficking into mitochondria but with a functional p21 pathway, with CCL660 (1.5 mg/Kg) *i.p.* twice a week for 8 weeks to investigate whether efficacious miR-660 delivery was achieved by increasing the duration of treatment and to confirm the dependency of the effects of CCL660 on the presence of a wild-type *P53* gene. Interestingly, a 50% reduction in the tumor volume was observed in treated mice compared with controls at 68 days (volume: 133 ± 15, 244.6 ± 38 and 250 ± 50 mm^3 in CCL660-treated, CCLSCR-treated and control tumors, respectively, $p < .05$; Fig. 3A and B). According to the dPCR data, CCL660 reached tumors, as a 7-fold increase in the miR-660 levels was observed in the treated groups compared with controls. Accumulation of miR-660 was also observed in the spleen, liver, lungs and plasma of treated mice (Fig. 3C). Furthermore, higher miR-660 expression was observed in the tumors using miRNA ISH (22%, 5% and 3% miR-660-positive cells in CCL660-treated and control tumors, respectively; $p < .05$) and a reduction in the number of Ki-67 positive cells in CCL660-treated tumors was observed using IHC (36% reduction in the number of Ki-67-positive cells compared with that in controls; $p < .05$; Fig. 3D and Fig. S2) were observed.

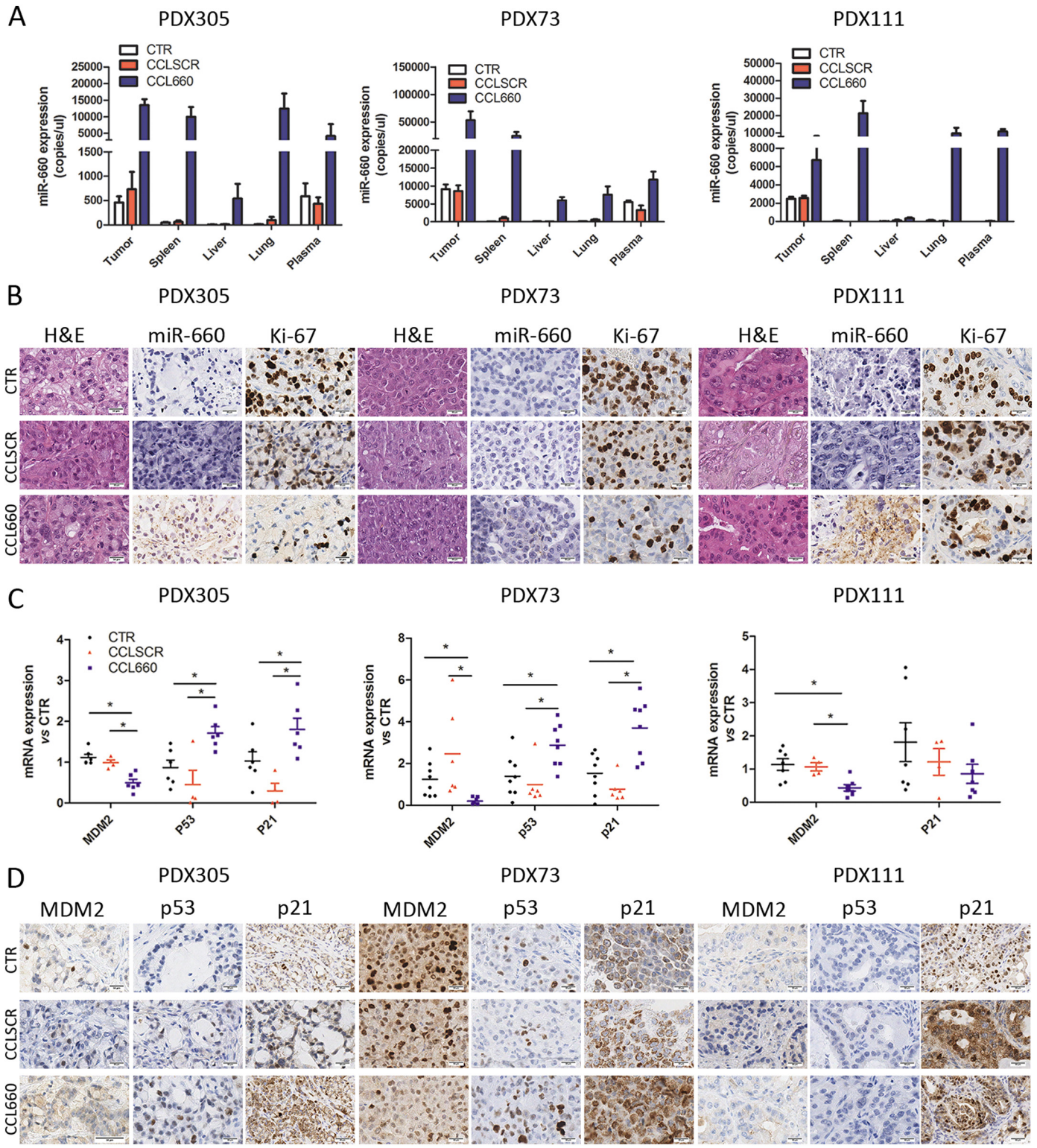

Fig. 2. CCL660 induces cell cycle arrest by modulating MDM2 expression. **A**) Graphs of dPCR data show miR-660 accumulation in tumors and other organs from mice transplanted with PDX305 (left panel), PDX73 (centre panel) and PDX111 (right panel). **B**) Representative images of miR-660 ISH and Ki-67 staining in PDX tumors after CCL660 treatment. **C**) Graphs of real-time PCR data show MDM2 down-regulation and increased *P53* and *P21* expression in PDX305 (left panel) and PDX73 (centre panel), whereas only reduced MDM2 expression was observed in PDX111 (right panel) (n = 6 for CTR and CCL660, n = 4 for CCLSCR for PDX305; n = 7 for CTR and CCL660, n = 6 for CCLSCR for PDX111 and n = 8 for CTR and CCL660, n = 6 for CCLSCR for PDX73). **D**) Representative images of MDM2, P53 and P21 staining in PDXs after CCL660 treatments (42 days). Data are presented as means ± S.E.M. * $p < .05$ (One-way ANOVA test comparing CCL660 *vs* CTR or CCLSCR).

CCL660 downregulated the expression of the *MDM2* mRNA, as assessed by real-time PCR, with concomitant increase in the transcription of *P53* and its effector, the P21 protein (Fig. 3E). Interestingly, a decrease in the levels of the MDM2 protein (44% reduction in MDM2 levels in treated mice compared to those in controls; $p < .05$) (Fig. 3F) and up-regulation of P53 and P21 protein were detectable by IHC after

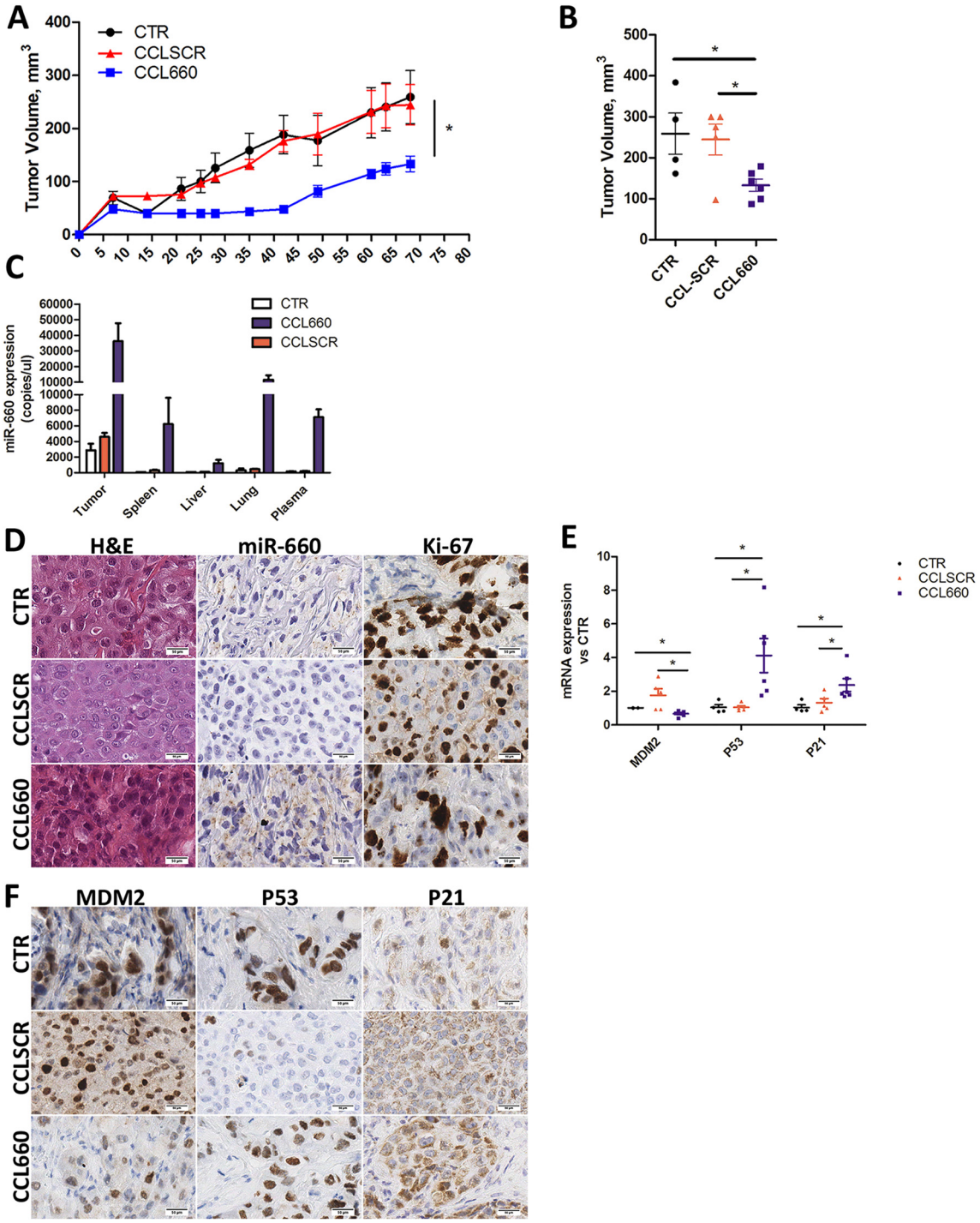

Fig. 3. Long lasting treatment increases the anti-tumor effects of CCL660. **A)** Tumor growth for PDX302 treated with CCL660 (1.mg/kg) for 8 weeks. The black arrow indicates the day on which treatment began. **B**) Graphs show reduced tumor volumes in CCL660-treated mice compared to those in CCLSCR and CTR mice. **C**) Graphs of dPCR data show miR-660 accumulation in tumors and other organs in treated mice. **D**) Representative images of miR-660 ISH and Ki-67 in PDX after CCL660 treatment. **E**) Real-time PCR data illustrating *MDM2* downregulation and increased *P53* and *P21* expression **F**) MDM2, P53 and P21 IHC expression on PDX treated with CCL660 or CCLSCR or CTR (n = 4 for CTR, *n* = 5 for CCLSCR and n = 6 for CCL660). Data are presented as means ± S.E.M. * $p < .05$ (One-way ANOVA test comparing CCL660 *vs* CTR or CCLSCR).

CCL660 treatment, supporting that hypothesis that miR-660 induced cell cycle arrest in tumor cells (Fig. 3F).

2.5. CCL660 does not induce side effects on normal tissues and cells

The evidence that CCL660 administration increased levels of miR-660 also in non-target organs, such as lung, liver and spleen, prompted us to investigate whether miRNA over-expression could have side effects on normal tissues. In this regard, it is worth mentioning that though human hsa-miR-660 is not conserved in the mouse, a murine miRNA having the same seed sequence as miR-660 exists, namely mmu-miR-6987 (Fig. 4A). The two miRNAs are hence expected to share part of their targets, provided that the latter have conserved binding sequences in their 3'UTRs. This is the case of *MDM2*, because murine

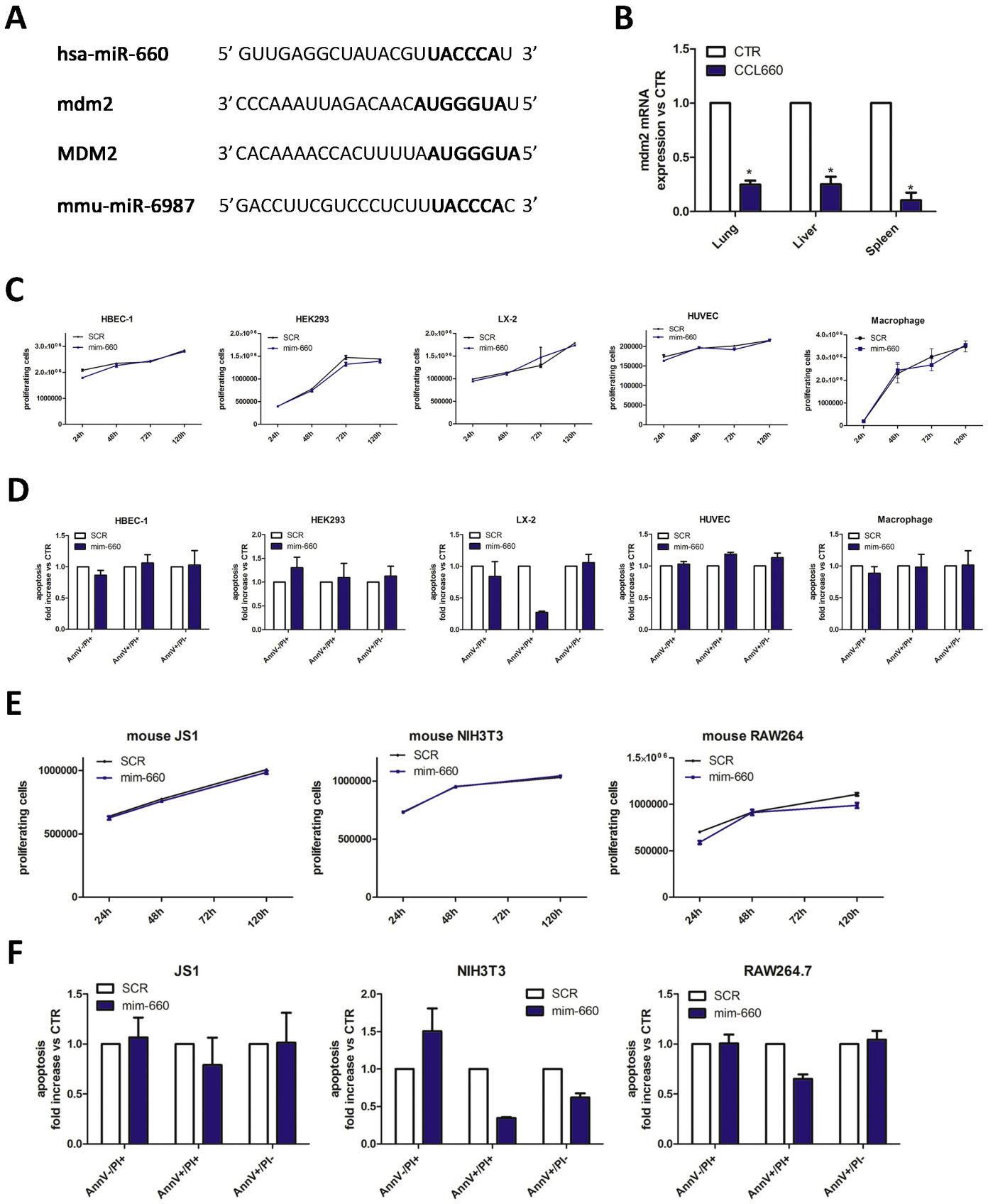

Fig. 4. MiR-660 did not induce side effects in normal tissues. A) Mdm2 3′ UTR-binding site for mmu-miR-6987. **B**) Mdm2 mRNA levels in mouse organs treated with CCL660 or control (n = 10). **C-D**) Proliferation (**C**) and apoptotic (**D**) graphs of human cell lines transfected with miR-660 or mimic control (50 nM, n = 5 for each assay). ***E*-F**) MiR-660 over-expression did not induce any changes of proliferation (**E**) and apoptosis (**F**) in murine cell lines. Data are presented as means ± S.E.M. * $p < .05$.

ortologue *Mdm2* is predicted to be target of both human miR-660 and murine miR-6987 (Fig. 4A). Since miR-660 could potentially bind murine *Mdm2*, we analyzed *Mdm2* mRNA expression in healthy tissues from mice treated with CCL660 and observed a statistical significant reduction of *Mdm2* expression in lung, liver and spleen (Fig. 4B). Despite this, CCL660 did not induce any major side effects on such organs, as evidenced by organ weight and immune cell infiltrates analysis performed after 4 weeks of CCL660 treatment in immunodeficient mice (Fig. S3A-B).

The safety of the cationic lipid DOTAP for the cells has been previously demonstrated *in vitro* and *in vivo* for asODNs and siRNAs [24,25,34,35]. To confirm the evidence that normal cells well tolerate miR-660 over-expression, we analyzed proliferation rate and apoptosis in various cell types both from human and mice after miRNA transfection. In particular, we selected non tumorigenic human bronchial epithelial cells (HBEC-1), human kidney cells (HEK293), human hepatic stellate cells (LX-2), human endothelial cells (HUVEC) and primary human macrophages from healthy donors.

As shown in Fig. 4C we did not observe any significative changes in cell proliferation at 72 and 120 h after miR-660 transfection for all the cells analyzed. Furthermore, we evaluated apoptosis by measuring the $AnnexinV^{pos}/PI^{neg}$ cells in miR-660 over-expressing cells without observing changes in the number of apoptotic cells after 72 h compared to cells transfected with mimic control (Fig. 4D). MiR-660 over-expression did not induce any significative changes in proliferation and apoptosis also in mouse liver, kidney and macrophage cells (Fig. 4E-F).

Overall, these findings let speculate that though CCL660 delivers miR-660 also to non-target organs and cells, normal cells are somehow tolerant to miR-660-induced *MDM2/Mdm2* down-regulation. Furthermore, our results show that MDM2 inhibition is selective and induces p53-dependent cell death only in tumor cells as already described for Nutlin and other small MDM2 inhibitors [36].

2.6. CCL660 does not induce immune-related toxic effects

It is known that liposomal compounds may have immune-related toxic effects [37]. To assess the acute *in vivo* toxicity of our lipidic vehicles we injected *i.p.* HEPES-buffered saline alone (CTR) or a single dose (1.5 mg/kg) of miR-660 or miR-SCR entrapped in lipidic nanoparticles (CCL660 or CCLSCR) into immunocompetent mice ($n = 3$ animals per group) and evaluated blood biochemistry, organ weight, immune cell infiltrates in organ tissues, and chemokine, cytokine and growth factor production [38].

As shown in Fig. 5A-B,H&E staining did not reveal any signs of inflammation in the organs, and no significant changes occurred in immune subpopulations in CCL660-treated mice compared with those in controls. Furthermore, no variations in the body and organ weights were observed in mice treated with lipid-nanoparticles, again confirming that our lipidic vehicles did not exert any apparent toxic effects.

Blood biochemical analyses of metabolites (alanine transaminase (ALT), aspartate transaminase (AST), azotemia, glucose and creatinine) did not reveal significant differences between CCL660 and the control (Table 2), indicating that lipid-nanoparticles did not exert toxic effects on the liver and kidney of treated mice.

We also performed a plasma cytokine array to detect levels of 22 pro-inflammatory cytokines, and no changes in the levels of these proteins were observed in mice treated with CCL660 or CCLSCR, excluding major effects of the lipid-nanoparticles on the activation of the immune system (Fig. 5C).

To exclude potential chronic toxic effects, we analyzed blood biochemistry, organ weight, immune cell infiltrates in organ tissues, and cytokines after 4 weeks of CCL660 treatment in immunocompetent mice ($n = 5$ animals per group).

The necropsy results did not reveal any macroscopic changes in the organs of mice after 4 weeks of CCL660 treatment and the results of the histopathological analysis and the organ weight assessments did not show changes in any of the mice treated with CCL660 (Fig. 4D-E). Blood metabolites and cytokine analysis did not reveal any modulations after nanoparticles treatments confirming the absence of chronic toxic effects of our compounds (Table 3 and Fig. 4F).

2.7. MiR-660 inhibits cancer growth in a lung colonization model

Since our PDXs models didn't disseminate efficiently to the lungs to form visible lung nodules [39], we established a lung colonization assay in immunocompromised mice to prove the efficacy of miR-660 in inhibiting lung cancer growth also in an orthotopic model of lung cancer. Specifically, we *i.v.* injected SCID mice with 1×10^6 H460 lung cancer cells that had been stably transfected with miR-660 (H460-miR-660) or a scrambled sequence (H460-miR-CTR) as a control, and monitored lung nodule growth using an ^{18}F-FDG animal PET analysis. Interestingly, 28 days after cells were injected, ^{18}F-FDG uptake was observed in the lungs of H460-injected mice, but not H460-miR-660 mice (Fig. 6A, upper panels). Moreover, an *ex vivo* PET analysis of mouse lungs showed decreased ^{18}F-FDG uptake in H460-miR-660-injected mice compared with that in H460 control-injected mice (Fig. 6A, lower panels). H&E and pan-cytokeratin staining confirmed a reduction in lung nodule growth in miR-660-overexpressing H460 tumors compared with that in controls (Fig. 6B-C). In fact, only one nodule was detected in the lungs of H460-miR-660-treated mice. Furthermore, we performed ISH to analyze the expression of miR-660 and observed that miR-660 was not expressed in H460-miR-CTR mice, whereas only a few miR-660 positive cells were observed in the treated group (Fig. 6B). IHC staining for MDM2 confirmed the inverse correlation between miR-660 expression and staining for the MDM2 protein. Interestingly, the lung nodules observed in H460-miR-660-treated mice did not express this miRNA in tumor cells and exhibited MDM2 levels similar to control cells, indicating that miR-660 expression was lost, allowing tumor growth in the lung (Fig. 6B-C).

3. Discussion

The rationale for the use of miRNA mimics in lung cancer is based on the evidence that miRNAs are deregulated and involved in lung cancer development [40] and that miRNA replacement in cancer cells reverts their aggressive phenotype [41]. As shown in our previous report, miR-660 is down-regulated in lung cancer tissues, and the over-expression of this miRNA in tumor cells reduces their migration and proliferation. The anti-tumor activity of miR-660 was mediated by down-regulating *MDM2* and restoring P53 function [18].

Here, lipid-nanoparticles delivery of miR-660 reduced the tumor growth of lung cancer PDXs by inducing cell cycle arrest in a P53-dependent manner. Interestingly, in a *P53*-mutated PDX model, we did not observe changes in tumor proliferation, although we observed reduced *MDM2* expression in the *P53* wild-type models, confirming the importance of a functional *P53* gene for the anti-cancer activity of miR-660. In particular, anti-tumoral effects of CCL660 on PDX302 carrying a *P53* mutation, suggested that miR-660 could be also used to treat *P53* mutated tumors with a functional p21 pathway.

In our previous study, H460 lung cancer cells injected *i.v.* into SCID mice invaded the lung parenchyma and produced fully developed nodules, starting from a particular cellular subset endowed with a high seeding potential [39]. Our preliminary data show in a similar lung colonization assay, that miR-660 counteracted H460 nodule formation, suggesting that either miR-660 has a role in the processes underlying nodule development after the seeding of tumor cells in distant organs or a direct effect on the seeding process of circulating cells.

Lipid-nanoparticle systems are one of the most promising vectors for miRNA delivery. However, cationic liposomes were reported to be highly immunogenic due to the interactions between the positively charged lipids and proteins. Interferon-γ responses have been described after liposomal treatments [42].

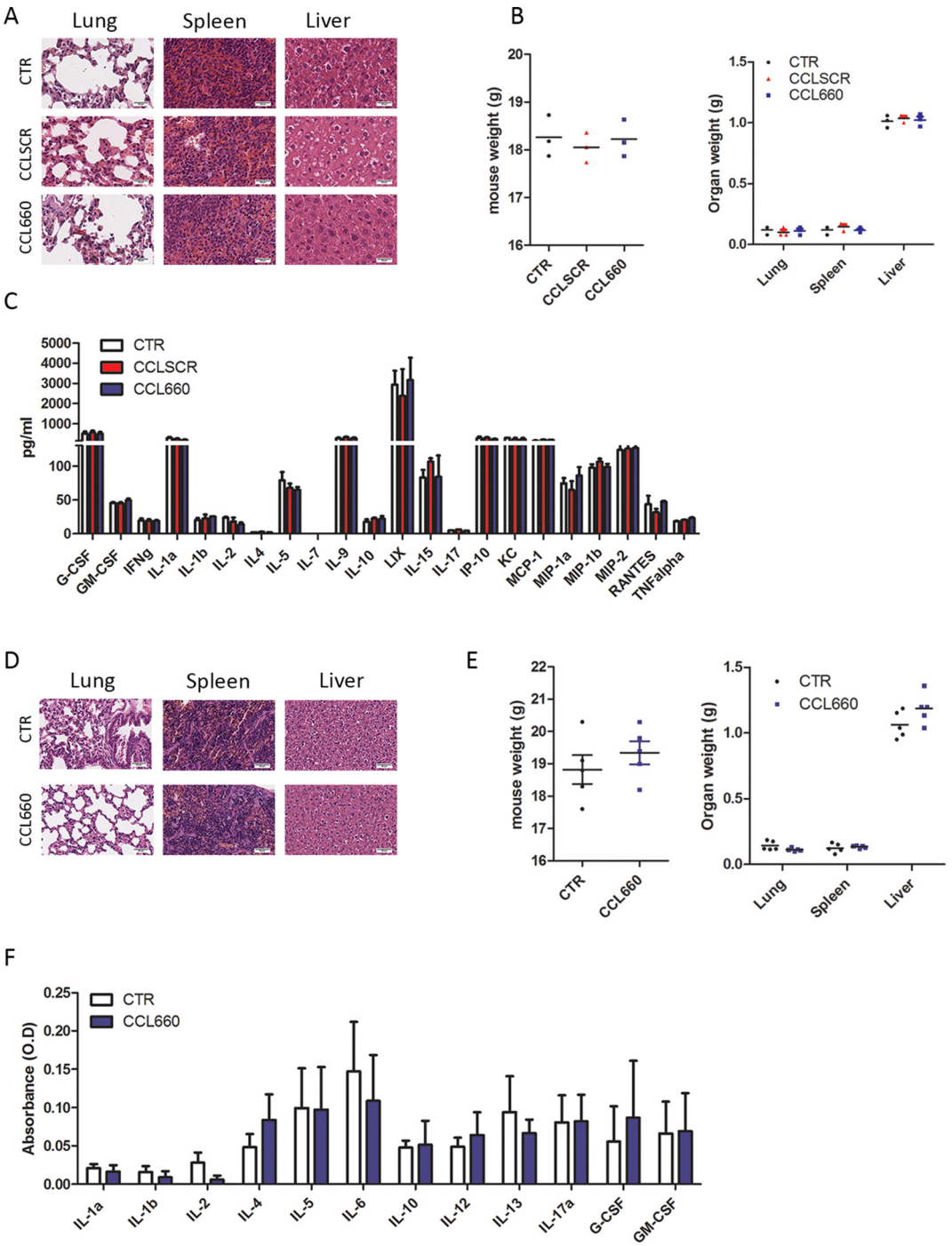

Fig. 5. CCL660 does not induce acute and chronic immune-related toxic effects. **A)** Representative H&E staining of immune infiltrates in mice injected with single dose (1.5 mg/kg) for 24 h of lipid-nanoparticles. **B)** Graphs show body and organ weights of CCLSCR- and CCL660-treated mice compared with controls. **C)** Bar graphs illustrate plasma pro-inflammatory cytokine levels in the CCL-treated mice ($n = 3$ mice per group). **D**) Representative H&E staining of immune infiltrates in mice injected with lipid-nanoparticles after 4 weeks of treatment. **E)** Graphs show body and organ weights of CCL660-treated mice compared with controls. **F)** Bar graphs illustrate plasma pro-inflammatory cytokine levels in the CCL660 (1.5 mg/kg) treated mice twice after 4 weeks of treatment (n = 5 mice per group). Data are presented as means ± S.E.M. * $p < .05$.

Evidence of miRNA replacement as an effective therapy for lung cancer in genetically modified mouse models was provided for let-7 and miR-34 [43], and the first compound based on miRNA mimics to enter a phase I clinical trial was MRX34, a liposomal miR-34 mimic compound tested in patients with liver cancer, other solid tumors and hematological diseases to assess pharmacokinetics and pharmacodynamics [44]. This trial was prematurely terminated because severe immune-related events causing patient deaths were recorded. The adverse events of MRX34 administration were related to pro-inflammatory changes and macrophage activation, which were potentially attributable to the liposome carrier and not the miR-34 mimics [45]. Based on this negative result, pre-clinical investigations of possible immune-related toxicity are required. Noteworthy, the lipid-nanoparticles herein used are a neutral lipid coated formulation identical, in the exterior surface, to that used to deliver asODNs, and siRNAs without any immunological-induced toxicities [24,25,34]. However, in the present study, we

Table 2
Acute liver and renal toxicity studies.

	AST[a] (IU/L)	ALT[b] (IU/L)	CRE[c] (mg/dL)	Azotemia (mg/dL)	Glucose (mg/dL)
CTR	123.5 ± 52.3	55.3 ± 17.8	0.02 ± 0.01	29.8 ± 3.6	111 ± 10.5
CCLSCR	116 ± 53	32 ± 17.01	0.021 ± 0.012	26.3 ± 1.4	119.5 ± 11.9
CCL660	82.3 ± 19.5	25 ± 15	0.019 ± 0.01	28.6 ± 5.2	114 ± 16.5

Blood samples collected 18 h after *i.p.* injections of CCLSCR or CCL660 or HEPES-buffered saline alone (CTR) were quantified to determine the serum levels of
[a] Aspartate Aminotransferase (AST),
[b] Alanine Aminotransferase (ALT),
[c] Creatinine (CRE), Azotemia and Glucose. Data are presented as means ± S.D.

Table 3
Chronic liver and renal toxicity studies.

	AST[a] (IU/L)	ALT[b] (IU/L)	CRE[c] (mg/dL)	Azotemia (mg/dL)	Glucose (mg/dL)
CTR	102.4 ± 43.9	67.3 ± 18.5	0.024 ± 0.017	32.8 ± 7.6	101.6 ± 26.8
CCL660	77.6 ± 15.1	60.3 ± 28.6	0.020 ± 0.003	31.6 ± 5.2	116 ± 2.2

Blood samples collected 16 h after the *i.p.* injection of 8 treatments (chronic toxicities) were quantified for serum levels of
[a] Aspartate Aminotransferase (AST),
[b] Alanine Aminotransferase (ALT),
[c] Creatinine (CRE), Azotemia and Glucose. Data are presented as means ± SD.

analyzed potential immune-related events after single or prolonged administration of CCL660 in immunocompetent mice, and did not observe modulation of acute inflammatory cytokines such as IFN-α or TNF-α compared to control animals. Long-term treatment of lipid-nanoparticles entrapping miR-660 didn't modulate plasma levels of several pro-inflammatory cytokines suggesting an absence of toxicity effects. Interestingly, histopathological analysis of the mouse organs after single and long-term treatments revealed that CCL660 didn't increase the immune cells infiltration in tissues excluding any signs of chronic toxicity.

Despite the encouraging results regarding toxicity, CCL660 only partially decreased tumor growth in *P53* wild-type PDXs, and miRNA ISH revealed that CCL660 only reached 30% of lung cancer cells, thus lacking a uniform distribution in the tumor samples. This low delivery efficiency, which is likely related to rapid clearance or phagocytosis of the liposomal compound by immune cells [37], could explain the limited inhibitory effects on tumor growth observed in our PDX models.

Lipid-nanoparticles represent an effective drug delivery system that is capable of altering the pharmacokinetic profile of a drug and delivering the encapsulated agent [46]. One potential strategy to improve the therapeutic efficacy of the miRNA mimics and to reduce non target toxicity is to modify lipid-nanoparticles by adding a tumor cell-specific ligand on the lipid surface.

Indeed, the combination of the pharmacokinetic advantages and tumor-selective biodistribution of lipid-nanoparticles with cell-specific binding and internalization induced by antibodies or receptor ligands is a recognized strategy to improve the therapeutic effectiveness of conventional chemotherapeutics or gene therapeutics for treating human malignancies, including lung cancer [26,47,48].

The availability of ligands or peptides or tumor-associated antigens would enable researchers to design more sophisticated cancer treatment strategies that exhibit high levels of selective toxicity for cancer cells [49].

Therefore, new candidate lung cancer cell-specific ligands must be identified to improve the therapeutic outcomes, decrease side effects and improve patients' quality of life.

Systemic delivery is the most feasible route for the use of miRNAs in the clinic, but the main challenge is the low uptake of the delivered miRNAs in lung cancer cells [50]. The development of new delivery systems, such as inhaled liposomes, may be a valid option to overcome this issue, particularly for lung cancer treatment [51]. The success of this method will depend on the development of new aerosol devices and the formulation of efficient inhalable liposomes.

Recently, the discovery that exosomes are secreted into body fluids and their ability to be loaded with miRNAs offered a new and interesting approach for miRNA delivery [52]. In addition, these microvesicles allow the cargo to escape from phagocytosis and are endowed with an increased half-life in the circulation compared to liposomes [53]. Thus, exosomes loaded with selected miRNAs represents an alternative and potentially valid therapeutic strategy for treating lung cancer.

Although challenges regarding efficient miRNA delivery persist, our experiments with lipid-nanoparticles entrapping miR-660 in preclinical mouse models showed promising results both in terms of tumor growth inhibition and the absence of toxic effects. However, future studies in pre-clinical models comparing the treatment with cationic lipid-nanoparticles carrying miR-660 with the standard of care for lung cancer patients or adding a tumor cell-specific ligand on the lipid surface to improve the therapeutic efficacy of the miRNA mimic and to reduce non target toxicity are needed. Overall, the present study provides new insights into the development of miRNA delivery systems as treatments for lung cancer.

4. Materials and methods

4.1. Reagents and chemicals

4.1.1. Lipids

Hydrogenated soy phosphatidylcholine (HSPC), cholesterol (CHE), 1,2-distearoylsn-glycero-3-phosphoethanolamine-N-[methoxy (polyethylene glycol)-2000] (DSPE-PEG2000), and 1,2-dioleoy-1-3- rimethylamonium propane (DOTAP) were purchased form Avanti Polar Lipids, Inc. (Alabaster, AL, USA).

miRVana™ miRNA Mimic Negative Control #1 (miR-NC1) and miRVana™ miRNA mimic miR-660 (miRNA ID# MC11216) for lipid-nanoparticles preparations were purchased from Ambion (Thermo Fisher Scientific, Waltham, MA, USA).

Nucleopore polycarbonate membranes were purchased from Avestin Inc. (Ottawa, ON, Canada). Sephadex G-50 was purchased from PerkinElmer Biosciences (Waltham, MA, USA).

All other reagents were of analytical grade or the highest available purity and were purchased from Sigma-Aldrich (St. Louis, MO, USA).

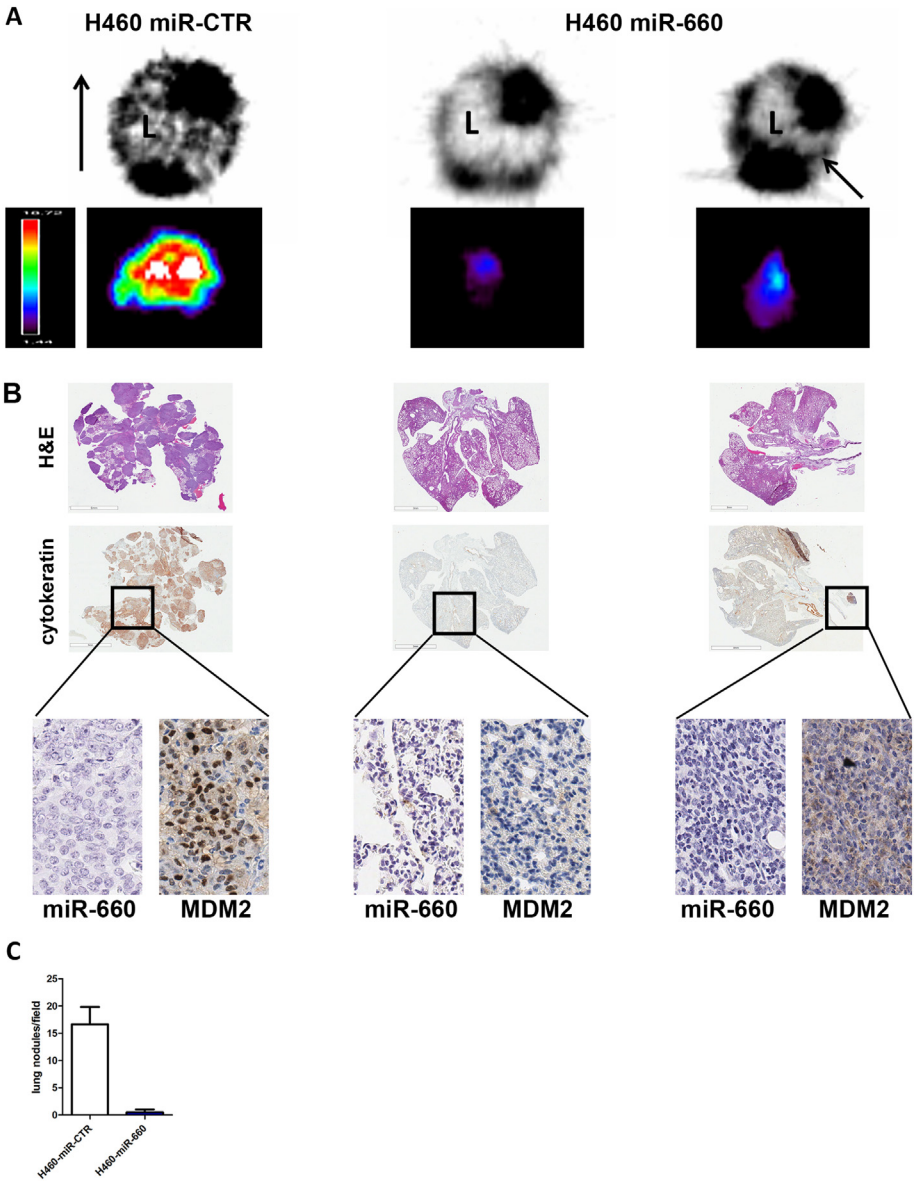

Fig. 6. MiR-660 inhibits cancer growth in lung colonization models. **A)** PET analysis of mice 28 days after the injection of 1×10^6 H460 lung cancer cells. **Upper panels** show representative axial sections of ^{18}F-FDG uptake in the lungs of mice injected with H460 (**left panel**) and H460-miR-660 cells (**middle** and **right panels**). H and L indicate the mouse heart and lung, respectively. **Lower panels** show the results of the *ex vivo* PET analysis of lungs from mice injected with H460-miR-CTR (**left panel**) and H460-miR-660 cells (**middle and right panels**). **B)** Representative images of H&E and pan-cytokeratin staining of the lungs from H460-miR-660-injected mice and control mice. The results revealed an inverse correlation between miR-660 and MDM2 levels in the lungs ($n = 2$ mice per group).

4.2. Cell lines

Human bronchial epithelial (HBEC-1), kidney (HEK293), hepatic stellate cells (LX-2), endothelial cells (HUVEC), H460 lung cancer, murine JS-1, NIH-3 T3 and RAW264.7 cell line (ATCC or Merck, USA) were cultured in appropriate medium. Primary human macrophages from healthy donors were obtained as described [54]. Stable miR-660-overexpressing H460 cells were obtained using methods described in a previous study [18].

4.3. Cells assay

Cells were seeded in a 6-well plate and transfected with 50 nM of miR-660 mimic or negative control (SCR) using Lipofectamine 2000 (Thermo Fisher Scientific) following manufacturer's protocols.

For proliferation assay cells were seeded in a 96 well plate at 2×10^3 cells and fluorescence were measured after 72 and 120 h using RealTime-Glo MT Cell Viability Assay (Promega). Each experiment was performed in quintuplicate.

Apoptosis was measured by quantifying the percentage of Annexin V^{pos}/Propidium $Iodide^{neg}$ cells by flow cytometry as previously described [18].

4.4. Preparation of CCLs

Small, stable Coated Cationic Lipid-nanoparticles (CCLs) entrapping miRNA-NC1 (CCLSCR) or miRNA-660 (CCL660) were prepared and purified as previously described [24,25]. Briefly, the DOTAP amount is modified according to the number of negative charges of synthetic antisense oligonucleotides, siRNA and miRNA [24,25,27,34]. Lipid-nanoparticles were sequentially extruded through 400 nm, 200 nm and 100 nm polycarbonate filters. Non-entrapped miRNAs were removed using a Sephadex G-50 column that had been pre-equilibrated with HEPES-buffered saline (25 mmol/L HEPES, 140 mmol/L NaCl, pH 7.4). The amount of miRNAs encapsulated in CCLs was evaluated by solubilizing lipid-nanoparticles preparations with 40 mmol/L sodium deoxycholate for 1.5 h at room temperature followed by spectrophotometer measurement at 260 nm [24,25]. The percentage of entrapped miRNAs was assessed by fluorescence-activated cell sorting (FACS) analysis as described and modified by us [24]. The particle size hydrophobic diameter (in nm), polydispersity index (PdI) and zeta potential (Z-potential in mV) of the lipidic nanoparticle preparations were measured using a Malvern Nano ZS90 light scattering apparatus (Malvern Instruments Ltd., Worcestershire, UK). The parameters set for analyses were a scattering angle of 90° and a temperature of 25°C

[24,25,29,55]. Z-potential values were recorded following dilution in distilled water or PBS. The results from the light scattering experiments are presented as average values of triplicate reading of each lipid-nanoparticle preparations used ± standard deviations.

4.5. PDXs and in vivo assays

PDXs were established as previously described [56]. Mice were maintained in the Animal Facility of Fondazione IRCCS Istituto Nazionale dei Tumori. Animal experiments were authorized by the Institutional Animal Welfare Body and Italian Ministry of Health and were performed in accordance with national laws (D.lgs 26/2014). Regarding the TP53 mutational status we profiled our PDX models and observed that PDX111 had P53p.C242X mutation whereas PDX302 had P53p.C135Y mutation that it is described a mutation important for mitochondrial trafficking of P53 [57].

Experiments were conducted using SCID mice (Charles River Laboratories, Lecco, Italy) bearing a PDX tumor in one flank. Mice were *i.p* or *i.v.* injected with 1.5 mg/Kg of the miR-660- or miR-SCR-entrapped lipid-nanoparticles (CCL660 or CCLSCR, respectively) or HEPES-buffered saline as the control (CTR) twice a week for four or eight weeks. Each time mice received a total volume of 200 μL of freshly diluted solution of lipid-nanoparticles in HEPES-buffered saline or 200 μL of HEPES-buffered saline alone. Dose and schedule of treatment was selected according to literature [58,59]. Tumor growth was monitored weekly using calipers, and the results were analyzed using GraphPad Prism 5 software (GraphPad Software, San Diego, CA, USA).

^{18}F-FDG PET analyses were performed on isoflurane-anesthetized SCID mice. Briefly, the mice were injected with 200 μL of ^{18}F-FDG (100 MBq) in an injectable solution. Forty-five minutes after the injection, the mice were analyzed using the PETGE Explore Vista system (General Electric Healthcare, Chalfont St. Giles, UK) for 20 min. At the end of the PET analysis, the mice were sacrificed, and lungs were removed and immediately analyzed for ^{18}F-FDG uptake *ex vivo*.

4.6. Analysis of miRNA and mRNA expression in tissues

PDXs and mouse tissues were first homogenized using 3 mm Tungsten Carbide Beads and the Mixer Mill MM300 (Qiagen, Hilden, Germany), and then total RNA was extracted using the automatic Maxwell RSC Instrument (Promega, WI, USA) and commercially available kits (Qiagen), according to the manufacturers' instructions. Next, 20 ng of total RNA were reverse transcribed into cDNAs by performing multiplex reverse transcription PCR (RT-PCR) using the TaqMan MicroRNA Reverse Transcription Kit (Thermo Fisher) and a TaqMan RT Primer Pool with the miRNAs of interest (Thermo Fisher). dPCR was performed as described by Conte et al. [60].

For gene expression analyses, reverse transcription was performed using 250 ng of total RNA. The TaqMan microRNA assay (Thermo Fisher) and ready-to-use Assay on Demand (Thermo Fisher) were used with a QuantStudio 7 Flex System (Thermo Fisher) to analyze the expression of selected genes, and the human GAPDH gene was used as a reference for sample normalization.

4.7. ISH analysis of miRNAs

The protocol for miR-660 ISH on PDX and mouse tissues is based on a combination of double DIG-conjugated mirCURY locked nucleic acid (LNA) probes (Exiqon, Vedbæk, Denmark) and a Tyramide Signal Amplification (TSA) DAB-chromogenic detection system (Perkin Elmer System) that together enable the specific and sensitive detection of miRNAs. Probe selected for ISH analysis is listed in Table 4. For image analysis, stained sections were examined under an optical microscope and scanned with AperioScanscope XT (Leica Biosystems, Nussloch, Germany). For miRNA quantification three random fields (Magnification: 30×) for each slides were analyzed counting the number of positive cells relative to the number of total tumoral cells.

Table 4
Detection probe.

Probe	RNA Tm[a] (°C)	T hyb[b] (°C)	Probe sequence
Hsa-miR-660	86	54	CAACTCCGATATGCAATGGGTA

[a] Tm: melting temperature;
[b] T hyb: hybridization temperature.

4.8. Immunohistochemical (IHC) staining

H&E staining and levels of the Ki-67 antigen and MDM2 protein were investigated using IHC. Briefly, 2.5/3 μm-thick sections were cut from paraffin blocks, dried, de-waxed, rehydrated, and unmasked (with Dako PT-link, EnVision FLEX Target Retrieval Solution, High Ph, Dako, Denmark). A Ki-67 monoclonal antibody (Clone MIB 1 Dako, dilution 1:400) and anti-MDM2 monoclonal antibody (Calbiochem; Merck Millipore; OP 46, dilution 1:60) were incubated in an automated immunostainer (DakoAutostainer System) using a commercially available detection kit (EnVision FLEX+, Dako). For each slide, positive cells were counted in 3 random fields at 30× magnification using an Aperio Scanscope XT (Leica Biosystems).

4.9. Determination of kidney and liver toxicity

Balb/c mice were purchased from Envigo (Envigo, S. Pietro al Natisone, Italy) and were housed under pathogen-free conditions; the experiments were reviewed and approved by the licensing and ethical committee of the IRCCS Azienda Ospedaliera Universitaria San Martino-IST Istituto Nazionale per la Ricerca sul Cancro (Genoa, Italy) and by the Italian Ministry of Health.

Mice were *i.p.* injected with a single dose (1.5 mg/Kg) of miR-660 or miR-SCR entrapped in CCL or HEPES-buffered saline alone (CTR). For chronic toxicity studies mice were treated *i.p*. twice a week for 4 weeks with 1.5 mg/Kg of CCL660 or HEPES-buffered saline alone. Each time mice received each times a total volume of 200 μL of freshly diluted solution of lipid-nanoparticles in HEPES-buffered saline or 200 μL HEPES-buffered saline alone. Eighteen hours after one or eight treatments, mice were sacrificed, blood was collected, and organs were excised. Livers, spleens, and lungs were weighed, fixed overnight with formalin, and then embedded in paraffin. Paraffin-embedded tissue sections were prepared as described above and then stained with H&E to evaluate the immune infiltrates in mice injected with lipid-nanoparticles.

Blood samples were harvested in tubes containing sodium citrate and then centrifuged at 1000 × *g* for 15 min at 4 °C. Plasma levels of Aspartate Aminotransferase (AST), Alanine Aminotransferase (ALT), Creatinine (CRE), azotemia and glucose were quantified as indicators of liver and kidney toxicity. The analyses were performed using the Cobas E6000 analyzer (Roche Diagnostics, Monza, Italy).

4.10. Cytokine, chemokine and growth factor quantification

The plasma derived from single dose -treated mice was also analyzed using the Bio-Plex Pro Assay (Bio-Rad Laboratories S.r.l, Milan, Italy) to determine the levels of the following cytokines: G-CSF (granulocyte colony-stimulating factor), GM-CSF (granulocyte-macrophage colony-stimulating factor), IFN-γ (*interferon gamma), IL-1α (*interleukin 1 alpha), IL-1β (interleukin 1 beta), IL-2 (interleukin 2), IL-4 (interleukin 4), IL-5 (interleukin 5), IL-7 (interleukin 7), IL-9 (interleukin 9), IL-10 (interleukin 10), LKI (lipopolysaccharide-inducible CXC chemokine), IL-15 (interleukin 15), IL-17 (interleukin 17), IP-10 (interferon gamma-induced protein 10), KC (mouse keratinocyte-derived cytokine), MCP-1 (monocyte chemoattractant protein 1), MIP-1α

(macrophage inflammatory protein 1 alpha), MIP-1β (macrophage inflammatory protein 1 beta), MIP-2 (macrophage inflammatory protein 2), RANTES (regulated upon activation, normal T cell expressed and secreted), and TNF-α (tumor necrosis factor alpha). The assay was performed using Luminex Technology by Bioclarma S.r.l. (Turin, Italy), according to the manufacturer's instructions.

Analysis of 12 cytokines levels (IL-1*α, IL-1β, IL-2, IL-4, IL-5, IL-6, IL-10, IL-12, IL-13, IL-17a, G-CSF, GM-CSF)* in plasma mice treated for 4 weeks with CCL660 or control was performed using Mouse Common Cytokines multi-Analyte ELISArray Kits following manufacturer's instruction (Qiagen). The absorbance at 450 nm was read using Infinite M1000 (Tecan, GmbH, Grodig/Salzburg, Austria).

5. Statistical analysis

Statistical analyses were performed using GraphPad Prism 5 software. Results are presented as mean values ± standard deviations (S.D.) and/or standard errors of the means (S.E.M.) for quantitative data. Statistical significance was determined using ANOVA with the Tukey's multiple comparison test, unpaired or paired *t*-tests. *P*-values $< .05$ were considered statistically significant.

Supplementary data to this article can be found online at https://doi.org/10.1016/j.jconrel.2019.07.006.

Competing Interest

We also declare that there aren't competing financial interests in relation to the work described.

Authors' contributions

O.F., M.Mo and D.D.P. designed the study; acquired, analyzed and interpreted the data; and drafted the manuscript. C.B., G.C., P.G., and V.B. acquired and analyzed the data. M.Mi., U.P., P.P., M.P., and G.S. designed the study, interpreted the data, and critically revised the manuscript. All authors approved the final version of the manuscript.

Declarations of Competing Interest

None.

Acknowledgments

The study was supported by grants from the Italian Association for Cancer Research [Investigator Grant Nos. 15928 to U.P., 14318 and 18812 to G.S., 14231 and 18474 to M.P., and 12162 to U.P. and G.S. (Special Program “Innovative Tools for Cancer Risk Assessment and early Diagnosis”, 5 × 1000)]; the Italian Ministry of Health [Grant No. RF-2010] and NIH/U01CA166905. O.F. was supported by the Cariplo Foundation Young Investigator Grant 2015 n.2015-0901. D.D.P. was supported by a Post-Doctoral Fellowship of Fondazione Umberto Veronesi. We thank Laura Emionite for providing technical assistance.

References

[1] M. Malvezzi, G. Carioli, P. Bertuccio, P. Boffetta, F. Levi, et al., European cancer mortality predictions for the year 2017, with focus on lung cancer, Ann. Oncol. 10 (2017).
[2] R.L. Siegel, K.D. Miller, A. Jemal, Cancer statistics, 2017, CA Cancer J. Clin. 67 (2017) 7–30.
[3] C. Zappa, S.A. Mousa, Non-small cell lung cancer: current treatment and future advances, Transl Lung Cancer Res 5 (2016) 288–300.
[4] J. Cosaert, E. Quoix, Platinum drugs in the treatment of non-small-cell lung cancer, Br. J. Cancer 87 (2002) 825–833.
[5] E.A. Collisons, B.S. Taylor, et al., Comprehensive molecular profiling of lung adenocarcinoma, Nature 511 (2014) 543–550.
[6] A.T. Shaw, D.W. Kim, K. Nakagawa, T. Seto, L. Crino, et al., Crizotinib versus chemotherapy in advanced ALK-positive lung cancer, N. Engl. J. Med. 368 (2013) 2385–2394.
[7] C. Gridelli, A. Rossi, D.P. Carbone, J. Guarize, N. Karachaliou, et al., Non-small-cell lung cancer, Nat Rev Dis Primers 1 (2015) 15009.
[8] M. Reck, D. Rodriguez-Abreu, A.G. Robinson, R. Hui, T. Csoszi, et al., Pembrolizumab versus chemotherapy for PD-L1-positive non-small-cell lung Cancer, N. Engl. J. Med. 375 (2016) 1823–1833.
[9] M. Reck, Pembrolizumab as first-line therapy for metastatic non-small-cell lung cancer, Immunotherapy 10 (2018) 93–105.
[10] A. Petitjean, M.I. Achatz, A.L. Borresen-Dale, P. Hainaut, M. Olivier, TP53 mutations in human cancers: functional selection and impact on cancer prognosis and outcomes, Oncogene 26 (2007) 2157–2165.
[11] Y. Haupt, R. Maya, A. Kazaz, M. Oren, Mdm2 promotes the rapid degradation of p53, Nature 387 (1997) 296–299.
[12] J. Momand, G.P. Zambetti, D.C. Olson, D. George, A.J. Levine, The mdm-2 oncogene product forms a complex with the p53 protein and inhibits p53-mediated transactivation, Cell 69 (1992) 1237–1245.
[13] U.M. Moll, O. Petrenko, The MDM2-p53 interaction, Mol. Cancer Res. 1 (2003) 1001–1008.
[14] C. Tovar, J. Rosinski, Z. Filipovic, B. Higgins, K. Kolinsky, et al., Small-molecule MDM2 antagonists reveal aberrant p53 signaling in cancer: implications for therapy, Proc. Natl. Acad. Sci. U. S. A. 103 (2006) 1888–1893.
[15] A. Esquela-Kerscher, F.J. Slack, Oncomirs - microRNAs with a role in cancer, Nat. Rev. Cancer 6 (2006) 259–269.
[16] M.V. Iorio, C.M. Croce, MicroRNA dysregulation in cancer: diagnostics, monitoring and therapeutics. A comprehensive review, EMBO Mol Med 4 (2012) 143–159.
[17] Z. Li, T.M. Rana, Therapeutic targeting of microRNAs: current status and future challenges, Nat. Rev. Drug Discov. 13 (2014) 622–638.
[18] O. Fortunato, M. Boeri, M. Moro, C. Verri, M. Mensah, et al., Mir-660 is down-regulated in lung cancer patients and its replacement inhibits lung tumorigenesis by targeting MDM2-p53 interaction, Cell Death Dis. 5 (2014) e1564.
[19] R. Rupaimoole, G.A. Calin, G. Lopez-Berestein, A.K. Sood, miRNA deregulation in Cancer cells and the tumor microenvironment, Cancer Discov 6 (2016) 235–246.
[20] J.F. Barger, S.P. Nana-Sinkam, MicroRNA as tools and therapeutics in lung cancer, Respir. Med. 109 (2015) 803–812.
[21] O. Fortunato, M. Boeri, C. Verri, M. Moro, G. Sozzi, Therapeutic use of microRNAs in lung cancer, Biomed. Res. Int. 2014 (2014) 756975(Epub;%2014 Sep 16.: 756975).
[22] V.P. Torchilin, Recent advances with liposomes as pharmaceutical carriers, Nat. Rev. Drug Discov. 4 (2005) 145–160.
[23] T.M. Allen, P.R. Cullis, Liposomal drug delivery systems: from concept to clinical applications, Adv. Drug Deliv. Rev. 65 (2013) 36–48.
[24] D. DiPaolo, C. Ambrogio, F. Pastorino, C. Brignole, C. Martinengo, et al., Selective therapeutic targeting of the anaplastic lymphoma kinase with liposomal siRNA induces apoptosis and inhibits angiogenesis in neuroblastoma, Mol. Ther. 19 (2011) 2201–2212.
[25] D. DiPaolo, C. Brignole, F. Pastorino, R. Carosio, A. Zorzoli, et al., Neuroblastoma-targeted nanoparticles entrapping siRNA specifically knockdown ALK, Mol. Ther. 19 (2011) 1131–1140.
[26] C. Brignole, F. Pastorino, D. Marimpietri, G. Pagnan, A. Pistorio, et al., Immune cell-mediated antitumor activities of GD2-targeted liposomal c-myb antisense oligonucleotides containing CpG motifs, J. Natl. Cancer Inst. 96 (2004) 1171–1180.
[27] P. Perri, D. DiPaolo, L. Priddy, A. Fiore, C. Brignole, et al., MicroRNA replacement and RNAi-mediated silencing of ALK as combined targeted therapies for neuroblastoma, Cancer Res Suppl 74: Meeting Abstract 1453, 2014.
[28] M. Moro, G. Bertolini, R. Caserini, C. Borzi, M. Boeri, et al., Establishment of patient derived xenografts as functional testing of lung cancer aggressiveness, Sci. Rep. 7 (2017) 6689.
[29] F. Piaggio, V. Kondylis, F. Pastorino, D. Di Paolo, P. Perri, et al., A novel liposomal Clodronate depletes tumor-associated macrophages in primary and metastatic melanoma: anti-angiogenic and anti-tumor effects, J. Control. Release 223 (2016) 165–177.
[30] M. Loi, P. Becherini, L. Emionite, A. Giacomini, I. Cossu, et al., sTRAIL coupled to liposomes improves its pharmacokinetic profile and overcomes neuroblastoma tumour resistance in combination with Bortezomib, J. Control. Release 192 (2014) 157–166.
[31] S.D. Li, L. Huang, Stealth nanoparticles: high density but sheddable PEG is a key for tumor targeting, J. Control. Release 145 (2010) 178–181.
[32] R. Rupaimoole, F.J. Slack, MicroRNA therapeutics: towards a new era for the management of cancer and other diseases, Nat. Rev. Drug Discov. 16 (2017) 203–222.
[33] M. Higashiyama, O. Doi, K. Kodama, H. Yokouchi, T. Kasugai, et al., MDM2 gene amplification and expression in non-small-cell lung cancer: immunohistochemical expression of its protein is a favourable prognostic marker in patients without p53 protein accumulation, Br. J. Cancer 75 (1997) 1302–1308.
[34] G. Pagnan, D.D. Stuart, F. Pastorino, L. Raffaghello, P.G. Montaldo, et al., Delivery of c-myb antisense oligodeoxynucleotides to human neuroblastoma cells via disialoganglioside GD(2)-targeted immunoliposomes: antitumor effects, J. Natl. Cancer Inst. 92 (2000) 253–261.
[35] C. Brignole, G. Pagnan, D. Marimpietri, E. Cosimo, T.M. Allen, et al., Targeted delivery system for antisense oligonucleotides: a novel experimental strategy for neuroblastoma treatment, Cancer Lett. 197 (2003) 231–235.
[36] S. Shangary, S. Wang, Small-molecule inhibitors of the MDM2-p53 protein-protein interaction to reactivate p53 function: a novel approach for cancer therapy, Annu. Rev. Pharmacol. Toxicol. 49 (2009) 223–241.
[37] C. Chakraborty, A.R. Sharma, G. Sharma, C.G.P. Doss, S.S. Lee, Therapeutic miRNA and siRNA: moving from bench to clinic as next generation medicine, Mol Ther Nucleic Acids 8 (2017) 132–143.

[38] X.D. Zhang, D. Wu, X. Shen, P.X. Liu, N. Yang, et al., Size-dependent in vivo toxicity of PEG-coated gold nanoparticles, Int. J. Nanomedicine 6 (2011) 2071–2081.
[39] G. Bertolini, L. D'Amico, M. Moro, E. Landoni, P. Perego, et al., Microenvironment-modulated metastatic CD133+/CXCR4+/EpCAM- lung Cancer-initiating cells sustain tumor dissemination and correlate with poor prognosis, Cancer Res. 75 (2015) 3636–3649.
[40] G. Sozzi, U. Pastorino, C.M. Croce, MicroRNAs and lung cancer: from markers to targets, Cell Cycle 10 (2011) 2045–2046.
[41] A.G. Bader, D. Brown, M. Winkler, The promise of microRNA replacement therapy, Cancer Res. 70 (2010) 7027–7030.
[42] D. De Paula, M.V. Bentley, R.I. Mahato, Hydrophobization and bioconjugation for enhanced siRNA delivery and targeting, RNA 13 (2007) 431–456.
[43] P. Trang, J.F. Wiggins, C.L. Daige, C. Cho, M. Omotola, et al., Systemic delivery of tumor suppressor microRNA mimics using a neutral lipid emulsion inhibits lung tumors in mice, Mol. Ther. 19 (2011) 1116–1122.
[44] A.G. Bader, miR-34 - a microRNA replacement therapy is headed to the clinic, Front. Genet. 3 (2012) 120.
[45] M.S. Beg, A.J. Brenner, J. Sachdev, M. Borad, Y.K. Kang, et al., Phase I study of MRX34, a liposomal miR-34a mimic, administered twice weekly in patients with advanced solid tumors, Investig. New Drugs 35 (2017) 180–188.
[46] D.C. Drummond, O. Meyer, K. Hong, D.B. Kirpotin, D. Papahadjopoulos, Optimizing liposomes for delivery of chemotherapeutic agents to solid tumors, Pharmacol. Rev. 51 (1999) 691–743.
[47] P. Sapra, P. Tyagi, T.M. Allen, Ligand-targeted liposomes for cancer treatment, Curr Drug Deliv 2 (2005) 369–381.
[48] F. Pastorino, D. Di Paolo, F. Piccardi, B. Nico, D. Ribatti, et al., Enhanced antitumor efficacy of clinical-grade vasculature-targeted liposomal doxorubicin, Clin. Cancer Res. 14 (2008) 7320–7329.
[49] F. Pastorino, C. Brignole, D. Di Paolo, P. Perri, F. Curnis, et al., Overcoming biological barriers in Neuroblastoma therapy: the vascular targeting approach with liposomal drug Nanocarriers, Small 15 (2019) e1804591.
[50] A.I. Minchinton, I.F. Tannock, Drug penetration in solid tumours, Nat. Rev. Cancer 6 (2006) 583–592.
[51] N.V. Koshkina, J.C. Waldrep, L.E. Roberts, E. Golunski, S. Melton, et al., Paclitaxel liposome aerosol treatment induces inhibition of pulmonary metastases in murine renal carcinoma model, Clin. Cancer Res. 7 (2001) 3258–3262.
[52] R.S. Conlan, S. Pisano, M.I. Oliveira, M. Ferrari, P.I. Mendes, Exosomes as reconfigurable therapeutic systems, Trends Mol. Med. 23 (2017) 636–650.
[53] S. Kamerkar, V.S. LeBleu, H. Sugimoto, S. Yang, C.F. Ruivo, et al., Exosomes facilitate therapeutic targeting of oncogenic KRAS in pancreatic cancer, Nature 546 (2017) 498–503.
[54] O. Fortunato, C. Borzi, M. Milione, G. Centonze, D. Conte, et al., Circulating mir-320a promotes immunosuppressive macrophages M2 phenotype associated with lung cancer risk, Int J Cancer, 2018.
[55] D. Di Paolo, F. Pastorino, G. Zuccari, I. Caffa, M. Loi, et al., Enhanced anti-tumor and anti-angiogenic efficacy of a novel liposomal fenretinide on human neuroblastoma, J. Control. Release 170 (2013) 445–451.
[56] M. Moro, G. Bertolini, M. Tortoreto, U. Pastorino, G. Sozzi, et al., Patient-derived Xenografts of non-small cell lung Cancer: resurgence of an old model for investigation of modern concepts of tailored therapy and cancer stem cells, J. Biomed. Biotechnol. 2012 (2012) 568567.
[57] W.M. Kamp, P.Y. Wang, P.M. Hwang, TP53 mutation, mitochondria and cancer, Curr. Opin. Genet. Dev. 38 (2016) 16–22.
[58] I.A. Babar, C.J. Cheng, C.J. Booth, X. Liang, J.B. Weidhaas, et al., Nanoparticle-based therapy in an in vivo microRNA-155 (miR-155)-dependent mouse model of lymphoma, Proc. Natl. Acad. Sci. U. S. A. 109 (2012) E1695–E1704.
[59] X. Huang, S. Schwind, B. Yu, R. Santhanam, H. Wang, et al., Targeted delivery of microRNA-29b by transferrin-conjugated anionic lipopolyplex nanoparticles: a novel therapeutic strategy in acute myeloid leukemia, Clin. Cancer Res. 19 (2013) 2355–2367.
[60] D. Conte, C. Verri, C. Borzi, P. Suatoni, U. Pastorino, et al., Novel method to detect microRNAs using chip-based QuantStudio 3D digital PCR, BMC Genomics 16 (2015) 849.